Efficient adsorption and removal of tetracycline antibiotics from aqueous solutions onto nickel oxide nanoparticles via organometallic chelate

Amnah Mohammed Alsuhaibani[a], Moamen S. Refat[b], A.A. Atta[c], M.G. El-Desouky[d,*], A.A. El-Bindary[e]

[a]Department of Physical Sport Science, College of Education, Princess Nourah bint Abdulrahman University, P.O. Box: 84428, Riyadh 11671, Saudi Arabia, email: amalsuhaibani@pnu.edu.sa
[b]Department of Chemistry, College of Science, Taif University, P.O. Box: 11099, Taif 21944, Saudi Arabia, email: msrefat@yahoo.com
[c]Department of Physics, College of Science, Taif University, P.O. Box: 11099, Taif, 21944, Saudi Arabia, email: a.atta@tu.edu.sa
[d]Egyptian Propylene and Polypropylene Company, Port Said 42511, Egypt, email: ch.moh.gamal@gmail.com ORCID Id: https://orcid.org/0000-0001-6060-463X
[e]Chemistry Department, Faculty of Science, Damietta University, Damietta 34517, Egypt, email: abindary@yahoo.com ORCID Id: https://orcid.org/0000-0002-4494-3436

ABSTRACT

In recent years, the use of antibiotics as a dietary additive to promote animal growth has significantly grown in both human and animal breeding. The identification of residues in water and wastewater is a result of this regular use. As a result, the creation of new bacterial strains that are resistant to these antibiotics has the potential to cause fatal livestock infections as well as the transmission of these strains to people. This research aims to utilize NiO nanosphere, which is produced through calcination of organometallic chelate. When employed as a tetracycline absorbent, 662 mg·g^{-1} of its strong adsorption capability were shown. Energy-dispersive X-ray spectroscopy, Fourier-transform infrared spectroscopy, and the generated NiO was examined using X-ray diffraction, including the 119.12 m^2·g^{-1} variable surface area for the Brunauer–Emmett–Teller model. Using scanning electron microscopy, it has become routine to measure surface changes. The tetracycline (TC's) capacity for adsorption under varied experimental circumstances (contact time, TC initial concentration, and pH values) was also examined. The developed adsorbent demonstrated improved TC adsorption capabilities at pH = 7, according to experimental results. The TC adsorption isotherms and kinetics best fitted Langmuir isotherm and pseudo-second-order model as the ($R^2 > 0.999$) for both models. The catalytic reduction of TC by NiO and the activation energy of 24.8 kJ·mol^{-1} both provided evidence that chemical reactions were primarily in charge of these processes. Additionally, by researching how temperature affects reactions, scientists can pinpoint thermodynamic variables like $\Delta G°$, $\Delta H°$, and $\Delta S°$ that confirm spontaneous endothermic reactions are more efficient at removing negative energy. Last but not least, the removal efficiency of TC in actual wastewater peaked at 97.6%, where even after 5 reuse cycles still maintained a commendable 93.6%.

Keywords: Adsorption; Kinetics; Isotherm; Thermodynamics; Tetracycline

* Corresponding author.

1. Introduction

The significance of organic contaminants in wastewater has grown during the past few years [1]. These contaminants, which include heavy metals, surfactants, dyes, and medications, can quickly harm the water and pose a risk to living things [2]. Furthermore, residual antibiotics have been discovered in groundwater and surface water across the globe [3,4]. Antibiotics are extensively employed in significant quantities to control diseases that affect organisms because of their effectiveness in treating infections-related ailments [5]. One of most crucial pharmacological antibiotics, tetracycline hydrochloride (TCN), is being used to treat a variety of diseases brought on by different types of pathogenic bacteria [6,7]. It has been used frequently to cure animal ailments, notably when it is added to animal feed to promote growth. It was discovered that TCN can enter the soil and aquatic ecosystem through application of organic fertilizers for plants because of its high solubility in water [8]. Since most of these antibiotics travel through organisms' bodies without being utilized in the metabolic activities and are then thrown into the environment, contaminated water sources result [9]. Despite the relatively low levels of antibiotics in surface and ground waters [10], they should not be ignored since their effects on the ecosystem are threatened by their continuous presence [11]. In order to avoid releasing antibiotic residue into the aquatic environment, it is vital to eliminate it from its primary sources [12,13].

Human progress in a variety of sectors, industry, agriculture, and other sectors produce enormous amounts of garbage that could be hazardous to both human health and the environment and have an effect on the economy [14]. Leading to significant pollution issues. Pollution of the air, water, and soil is caused by improperly managed wastes. Waste storage-related soil contamination may result in groundwater contamination from landfill leachate leaks [15,16].

The landfill is a sophisticated reactor that advances on its own. A complicated reactor that progresses spontaneously is a landfill. The following xenobiotic substances can be recognised in the effluent despite its complexity: tetracycline, pesticides, plasticizers, chlorinated aliphatic compounds, aromatic hydrocarbons, and phenols. Antibiotics have been found in leachates among other substances. Tetracycline, chlorinated aliphatic chemicals, aromatic hydrocarbons, phenols, insecticides, and plasticizers can all be distinguished from the effluent despite its complexity. Antibiotics were found among the substances in leachates [17,18]. Antibiotics have been found in leachates among other substances. In sewage treatment facilities, the municipal effluents that contained these molecules were cleaned before being released into surface waters (stream, sea) [19,20]. These residues were dispersed and maintained in the sludge before being dumped on the land. Groundwater serves as the primary receiving environment for a stand-alone purification system.

Antibiotics have been found in leachates amongst many other substances. These substances were used to cure pathogenic disorders in both humans and animals, and their usage has significantly expanded in recent years to protect those who are sensitive from bacterial infections. They were also employed as a growth hormone for agricultural animals [21–23]. Following administration, antibiotics were generally altered in both human and animal bodies. Their main methods of elimination were through the urine and faces, either through the original chemical or metabolites (molecule that is created from the inclusion of the parent molecule via oxidizing or conjugation in the body). Municipal discharges containing these molecules were cleaned up in sewage treatment facilities before being discharged into surface waters. These wastes were dispersed and part of them were maintained in the sludge before being dumped on the land. Groundwater serves as the main collect environment for a particular purification procedure [24–26]. Antibiotics become ineffective when used inappropriately and without cause, which results in the creation of resistance of microorganisms [27–29]. As a result, the tetracycline was chosen because of its ability to penetrate both soil and aquatic environments [30]. On the soil, tetracycline residues were frequently found [31], sediments [32], surface water, in the groundwater [33], wastewater. Numerous methods, including ozonation, have been used to remove different antibiotics from aqueous solutions [34–36], modern oxidation techniques, deterioration caused by photocatalysis [37,38], coagulation [39,40], and adsorption. Nevertheless, it has many challenges, such as poor performance, challenging operation, and harmful by-product production [41,42]. Adsorption has the most promise between these techniques due to its simplicity in manufacturing, low cost, and high efficacy, and lack of harmful intermediates. Water contaminants like activated carbon, metal oxides, clays, and agricultural wastes have all been removed using a variety of adsorbents. Furthermore, because natural adsorbents are inexpensive, researchers are concentrating on how widely they are used in water treatment [43]. Due to the π–π interaction, H-bond, and π-cation-bond that exist between tetracycline (TC) and metal oxide materials, they have lately been used as the most effective adsorbents [44].

Creating successful treatment technologies to get rid of impurities is becoming more and more important. The need for successful treatment methods to get rid of pollutants is still quite great. Technical landfills are designed to store final waste while reducing pollution and environmental hazard issues. This project sought to create effective composite geomaterials for the eradication of persistent organic pollutants [44,45].

This research was done to find out how NiO nanoparticles work together to help tetracycline bind to surfaces in aqueous solutions. The NiO created in this work was designed for waste containment. It was simply synthesized and described, giving it a large surface area of 119.12 $m^2 \cdot g^{-1}$ and efficiently removing TC from waste water at a rate of 662 $mg \cdot g^{-1}$. Additionally, these nanocomposite materials can be recycled after being utilized around five times. The reaction was endothermic and spontaneous, as the effect of temperature showed on other hand, the adsorption isotherm was fitted to Langmuir while the adsorption kinetic and kinetic was fitted to pseudo-second-order.

2. Material and methods

Prepared previously and illustrated at supplementary material [46].

2.1. Preparation of NiO nanoparticles

The NiO was obtained by calcination of $[Ni(L)Cl(OH_2)_3]$ H_2O chelate at temperatures of 450°C, 550°C, and 650°C for 4 h. This method produces NiO nanoparticles quickly and easily, without the use of expensive and harmful solvents or complicated equipment [47].

2.2. Preparation of adsorbate

Tetracycline with concentration (1×10^{-3} mol·L^{-1}) of was prepared using bi-distilled water during the preparation of the stock solutions and during the experimental study (Table S1).

2.3. Characterization of NiO

The devices and related models are illustrated in Table S2.

2.4. Batch adsorption studies

Experimentation with pH 2–12 and other factors were studied by dissolving a sufficient a certain amount of TC in distilled water, the effects of sorbent (NiO) dose concentration 0.01–0.1 g/25 mL, the effect of NiO dosage on the adsorption of (TC) in aqueous system and temperature (25°C–55°C) was examined [48–50]. Subsequent agitating at 200 rpm for 120 min, NiO was isolated by centrifugation. UV-Vis at 445 nm was used to assess the dye concentration. The proportion of decolorization (R) was determined from Eq. (1) (Table S3):

$$R = \frac{(C_0 - C_t)}{C_0} \times 100 \tag{1}$$

The adsorption potential (q_e, mmol·g^{-1}) was determined using the equilibrium Eq. (2):

$$q_e = \frac{(C_0 - C_e)V}{M} \tag{2}$$

3. Results and discussion

3.1. Characterization of NiO nanoparticles

3.1.1. X-ray diffraction patterns

Fig. 1 displays the NiO X-ray diffraction (XRD) data at various calcination temperatures. The discovered NiO diffraction peaks show how the tetragonal structure developed in relation to the lattice constants; $a = b = 2.977$ Å, $c = 11.445$ Å, $\alpha = 90.0°$, $\beta = 90°$ and $\gamma = 120°$. That indicate the existence of NiO in triagonal from. The interplanar spacing (d_{hkl}) and Miller indices (hkl) for NiO are recorded in Table 1 (space group P3m1, (JCPDS card no.04-0835). Also, correspond to NiO (PDF#01-1239). No extra peaks due to contamination were detected, this considered great evidence of the synthesized NiO's high purity. Also, the identical XRD patterns of the NiO samples at various

temperatures may be seen. The crystal planes (111), (200), (220), (311), and (222) of bulk NiO can be easily indexed at 2θ = 37.20°, 43.20°, 62.87°, 75.20°, and 79.38°, respectively. By using Scherer formula Eq. (3) the crystallite size (D, Å) of the NiO nanoparticles was calculated.

$$D = \frac{K\lambda}{\beta \cos \theta B} \tag{3}$$

The high-intensity (200) peak was used to measure the NiO crystallite size was 28, 46, and 62 nm at the temperatures 450°C, 550°C, and 650°C, respectively. The average grain size increases and the specific surface area decreases as the temperature rises, which is easily determined [48,51]. The greater extent of NiO particle formation can be used to explain these findings [52,53].

3.1.2. Fourier-transform infrared spectroscopy pattern of nickel oxide nanosphere

The band observed at 1,638 cm^{-1} is because of the water's OH bending. A strong band at 610 cm^{-1} is assigned to the Ni–O stretching band which is consistent with that reported elsewhere confirm the formation of NiO nanoparticles. Due to adsorption of CO band at 1,127 cm^{-1} (C–O) and a symmetric stretching vibration at 1,249 cm^{-1} (COO^{-1}) appeared [48] Fig. 2.

Fig. 1. XRD of NiO nanoparticles.
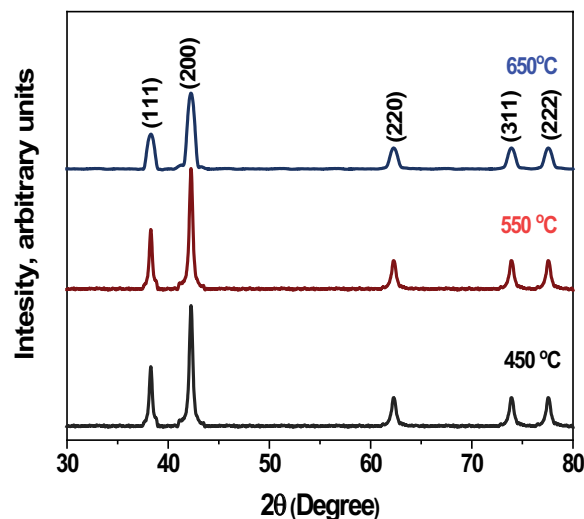
Table 1
Crystallographic of NiO

$2\theta_{Obs.}$ (°)	$2\theta_{Calc.}$ (°)	$d_{hkl(Obs)}$ (Å)	$d_{hkl(Calc.)}$ (Å)	(hkl)
38.279	37.984	2.3512	2.3688	012
42.259	37.984	2.1386	2.3688	012
62.295	61.26	1.4904	1.5131	110
73.935	74.394	1.2819	1.2751	202
77.575	78.064	1.2306	1.2241	018

3.1.3. Brunauer–Emmett–Teller surface area

Because the size and number of pores can significantly affect a substance's properties and its capacity for process, in a porous material [54,55]. It is crucial to calculate the holes' specific surface area. This is commonly accomplished by measuring the material's Brunauer–Emmett–Teller (BET) area of contact. Surface interactions occur whenever a gas comes into contact with the surface of a substance. The basis of BET tests is an adsorption isotherm that takes into account physisorption and the probability of a gas weakly adhering to a product's surface. Because physisorption is reversible, a gas can swiftly adsorb on to and desorb from a substance's surface.

The adsorption isotherm, which measures volume, is what happens when gas is adsorbs at various pressures while maintaining a constant temperature. Since liquid nitrogen is used to keep the temperature stable, it is around 77 K at this point. The complete adsorption isotherm graph can be produced by plotting the amount of gas adsorbed against the relative pressures. Curves shape of the plot shows the type of porosity existing at substance (Fig. 3) as well as the sort of pores in the substance (Fig. 4) (Table 4). The presence of a hysteresis loop is shown by type IV adsorption isotherms for NiO restricted absorption at high initial P/P_o and capillary condensation in a mesoporous medium the first loop is responsible for mono-multilayer adsorption, while the second is responsible for desorption. Adsorption effectiveness of the sample calcined at 450°C is higher in our case. Which has a lower crystallite1 size and a larger specific surface area than the others (119.12 m²·g⁻¹), pore size 6.07 nm which according to IUPAC it will be classified as mesoporous and pore volume 0.36 cm³·g⁻¹. and after adsorption of TC the surface area become 94.2 m²·g⁻¹ while the pore volume was 0.12 cm³·g⁻¹ these indicate the adsorption of TC take place through the pore filling of NiO [56].

3.1.4. Scanning electron microscopy analysis

Scanning electron microscopy (SEM) has been used to examine the surface properties of NiO nanoparticles (Fig. 4 shows consistent metal oxide formation) [57–59].
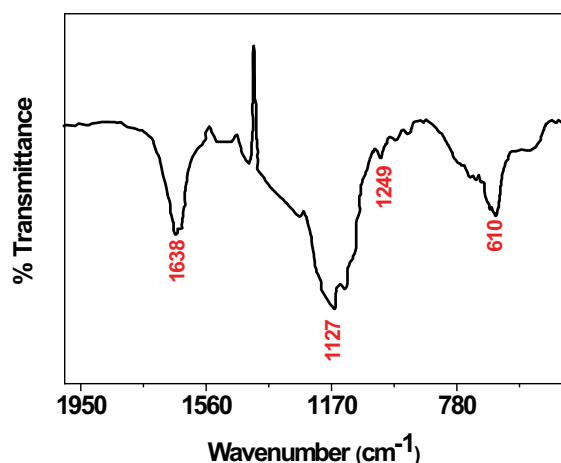
The cultivated nanostructures are in the form of nanoparticles that were interlinked and created pores and fissures, resulting in vast surface areas for rapid dye dispersion on metal oxide surfaces, SEM photos at greater microscopy demonstrate this. NiO nanoparticles having a diameter ranging from 27 to 47 nm were approved by SEM examination [60,61].

3.1.5. Energy-dispersive X-ray spectroscopy

Owing to its atoms, each material will have its X-ray spectrum with its unique set of peaks, according to energy-dispersive X-ray analysis. Energy-dispersive X-ray spectroscopy (EDX) analyses was used to assess the compositions chemically of nanoparticles. Peaks for Ni and O were discovered, but no peaks for impurities, suggesting that NiO had been clean for a long period (Fig. 5) [60].

3.2. Batch experiments

3.2.1. Effect of pH

Fig. 7 illustrates TC absorption onto NiO as a function of pH in the starting solution (1.2×10^{-3} mol·L⁻¹, 25°C and
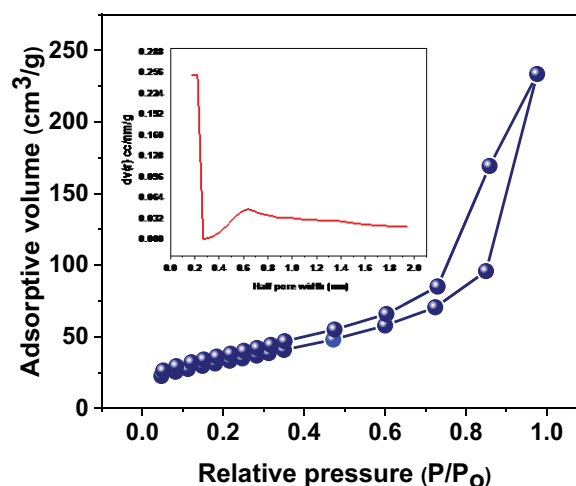

Fig. 3. NiO adsorption/desorption isotherm at 450°C for N₂.

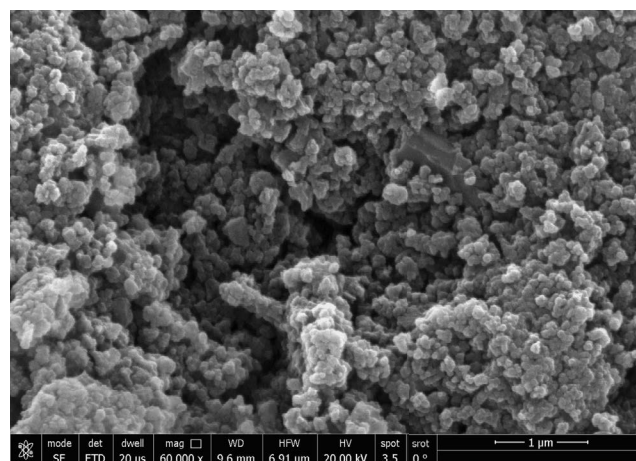Fig. 2. Fourier-transform infrared spectroscopy pattern of nickel oxide nanoparticles.

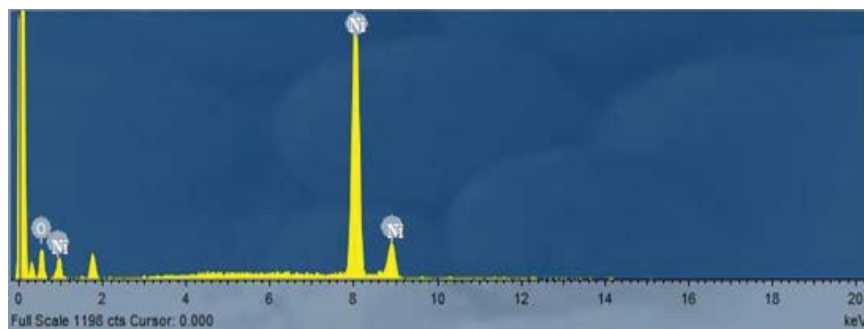Fig. 4. NiO nanoparticles as seen with a scanning electron microscope.

Fig. 5. NiO nanoparticles' EDX spectrum.

dosage 0.02 g/25 mL, contact time 60 min). A low pH seems to be the most effective for TC adsorption. Fig. 6 shows the impact of pH change on TC absorption onto NiO surface. Lower pH levels would cause hydrogen ions H$^+$ to adhere to the NiO surface, increasing the positively charged surface of the NiO. Therefore, the adsorption effectiveness may be reduced by the TC's electrostatic attraction on the NiO surface. Under normal circumstances, the opposite is true, where the NiO surface and H$^+$ divide, making the clay surface more negative. Therefore, the TC's electrostatic attraction to the negatively charged NiO surface can reduce the antibiotic's uptake level [62,63].

Furthermore, the increased adsorption efficiency may be reached at a pH of 7, which is somewhat near to the pH of the TC solution used in this investigation, which has a pH of about 7. The antibiotic is expressed as H3TC at this pH, which reduces the inhibitory electrostatic repulsion. This suggests that very acidic or basic environments were not preferred for TC adsorption; Consequently, all solutions were evaluated at pH 7, which is thought to be the average value of TC in an aqueous medium [64,65].

3.2.2. Effects of calcination

The influences of NiO calcination temperatures of 450°C, 550°C, and 650°C on TC adsorption studies were investigated. NiO dose was 0.02 g; the volume of dye solution was 25 mL; and concentration was 1.2×10^{-3} mol·L^{-1}, the pH level was 7, and the shake velocity was 200 rpm. The effectiveness of NiO adsorption increased when the calcination temperature was lowered 1.239 > 1.38 > 1.4516 mmol·g^{-1} for NiO at calcination temperature 450°C, 550°C and 650°C, respectively (Fig. 7) [66,67].

3.2.3. Influence of NiO dosage

By varying the adsorbent ranges, the TC adsorption of on NiO nanoparticles substance was investigated (0.01–0.1 g) per 25 mL, TC concentration of 1.51×10^{-3} mol·L^{-1} at 25°C and pH 4. The graph below shows how much of the entire amount of adsorbent TC can absorb (Fig. 8) [68]. Capacity of TC adsorption reduces as the dosage of NiO is raised 1.06 to 0.28 mmol·g^{-1} and rises from 0.01 to 0.1 g/25 mL. Fig. 9 depicts the influence of nickel oxide dose on the optimal concentration (C/C_0) of TC. As the dosage is increased while the adsorbent surface area is increased, the equilibrium concentration of (TC) decreases [69].
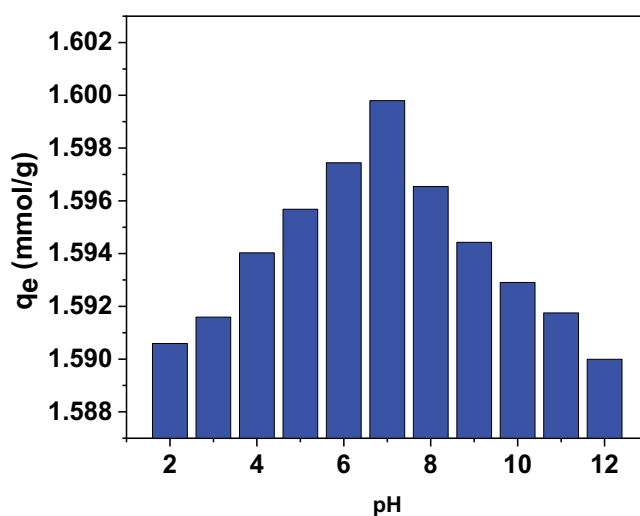

Fig. 6. Impact of pH on TC's adsorption on NiO.

3.2.4. Adsorption isotherms

TC absorption on NiO was computed utilizing isotherm models such as Langmuir [70], Freundlich [71], Temkin [72], Dubinin et al. [73]. Best fit was picked based on the R^2 about one. The results of the isotherm modelling are illustrated in Table 2. Langmuir isotherm model the best fit (Fig. 9). This shows that there is an active monolayer adsorption process. The monolayer adsorption potential was 1.527 mmol·g^{-1} (q_m) and 24.8 kJ·mol^{-1} is average sorption energy value [74]. In respect to the chemisorption process that has been suggested, this is accurate. Indeed, the limit energy for separation is generally agreed to be 8 kJ·mol^{-1}. Chemical sorption up to 8 kJ·mol^{-1} and physical sorption below 8 kJ·mol^{-1} [75–77].

3.2.5. Adsorption kinetics and mechanism studies

Uptake TC onto NiO was modeled using the pseudo-first-order [80], pseudo-second-order [81], intraparticle diffusion, and Elovich kinetic models in this study. The coefficient of determination (R^2) value was used to find the best fit. The pseudo-first-order and pseudo-second-order models were unable to specify governing diffusion mechanisms, hence an intra-particle mass transfer diffusion model utilized instead [82,83].
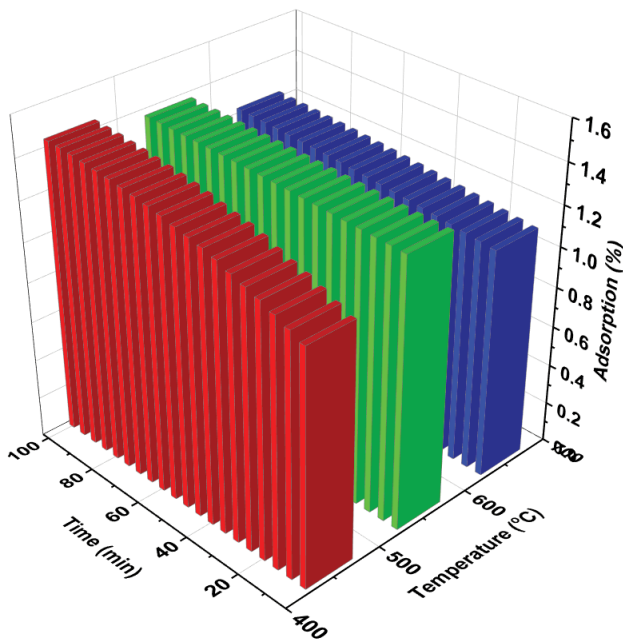
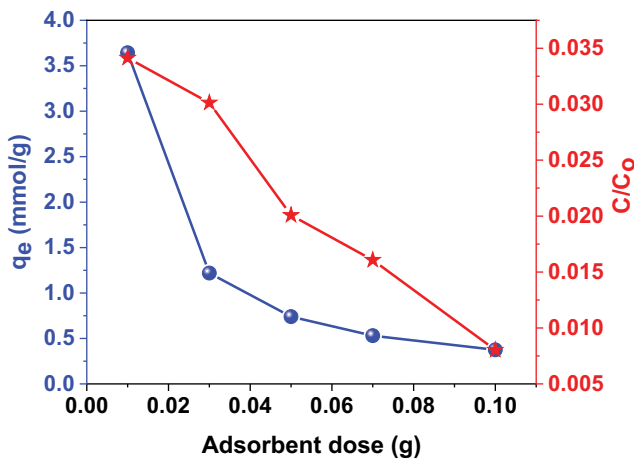Fig. 7. Impact of NiO calcination temperature on TC adsorption.

Fig. 8. Following are the effects of NiO dosage on TC adsorption: capacity of absorption vs. NiO dosage and relative residual concentration (C/C_0) vs. NiO dose.

Table 3 summarizes the findings of the kinetics modeling and displays the intraparticle diffusion equilibrium constant (K), pseudo-first-order constants (K_1), and pseudo-second-order constants (K_2). Due to its properties, For the adsorption mechanism, the pseudo-second-order is the ideal fit R^2 equals 0.999 is comparatively a greater correlation coefficient (R^2). Designates in the kinetics of absorption, the accessibility of binding sites as well as the quantity of dye in liquid are important considerations. The intraparticle diffusion kinetic modeling ($R^2 = 0.1999$) for TC calculated using the slope of the second linear region that corresponds in (Fig. 10). Early in the process of adsorption, the external barrier to mass transfer around the particles is crucial (initial sharp rise). The second equation portion intraparticle diffusion technique for continuous adsorption. If the plots not

intersect at beginning, this demonstrates that porosity dispersion not only rate-limiting stage; Extra simulations can control the adsorption rate as well, which are both capable of working in tandem [62,84]. As the adsorption sites of NiO heterogeneous, Elovich equation suggests a wide variety of activation energies for chemisorption. Parameter α (associated to the proportion of chemisorption). As the amount of dye in the solution increases, the parameter (which was proportional to the coverage surface) reduced (Table 3), this is because the useful adsorption surface of the adsorbate has decreased [85]. As a result, by raising the concentration within the range under study, chemisorption can occur more quickly. The excellent accuracy of the pseudo-second-order kinetic model makes it useful for simulating adsorption kinetics. It is predicated on the notion that the frequency step is electrostatic chemisorption because the adsorbent and the adsorbate share or exchange electrons [86,87].

3.2.6. Thermodynamic modelling studies

The change in free energy ($\Delta G°$), enthalpy ($\Delta H°$), and entropy ($\Delta S°$) computed using thermodynamics modeling to investigate several characteristics of NiO's adsorptive elimination of TC. Table 6 provides an overview of the results of thermodynamic modelling at many temperatures. As ($\Delta G°$) is negatively, the process is both possible and randomized ($\Delta G°$) values fell from –8.27 to –11.23 kJ·mol^{-1} at elevated temperature. As a result, the removal of TC from NiO becomes more appealing. Plotting ($\Delta G°$) against T's temperature reveals that it is linear (Fig. 11) ($\Delta H°$), and ($\Delta S°$) 26.35 and 0.118 kJ·mol^{-1}, respectively, were determined [88]. Positive $\Delta H°$ values demonstrate the endothermic nature of the adsorption mechanism. A positive value of ($\Delta S°$) identifies the existence of structural reforms on the NiO throughout absorption of TC. At the solid-liquid interface, randomization is becoming more prevalent. The good result also implies that the NiO adsorbent has a high affinity for TC [78].

The adsorption cycle's slope and intercept were calculated using the lnK_c vs. 1/T plot's standard ($\Delta H°$) and ($\Delta S°$) was determined. Arrhenius plot intercept was used to compute E_a (Fig. 12). The amount of $\Delta H°$ in adsorption processes is positive, indicating an endothermic reaction. While ($\Delta G°$) negatively, it designates spontaneous reaction (Table 4) [62]. In this scenario, the zero standard free energy temperature (T_0) is calculated to be 223 K for TC. The low T_0 values show that the tested adsorbents are functional and can absorb colourants at very low temperatures.

3.2.7. Mechanism of interaction

The largest amount of TC is absorbed when the pH reaches 7. Surface hydrogen bonding between TC and NiO may be able to explain this TC absorption, as an alternative, a pseudo-second-order kinetic model based on intra-particle diffusion is used. The chemistry of the NiO surface and the characteristics of the ionized adsorbate molecules may be impacted by the sorption solution's initial pH, which could be the cause of the observed phenomenon. The energy of the interaction between the charged TC molecule and the charging NiO surface may be one of the key operating factors.
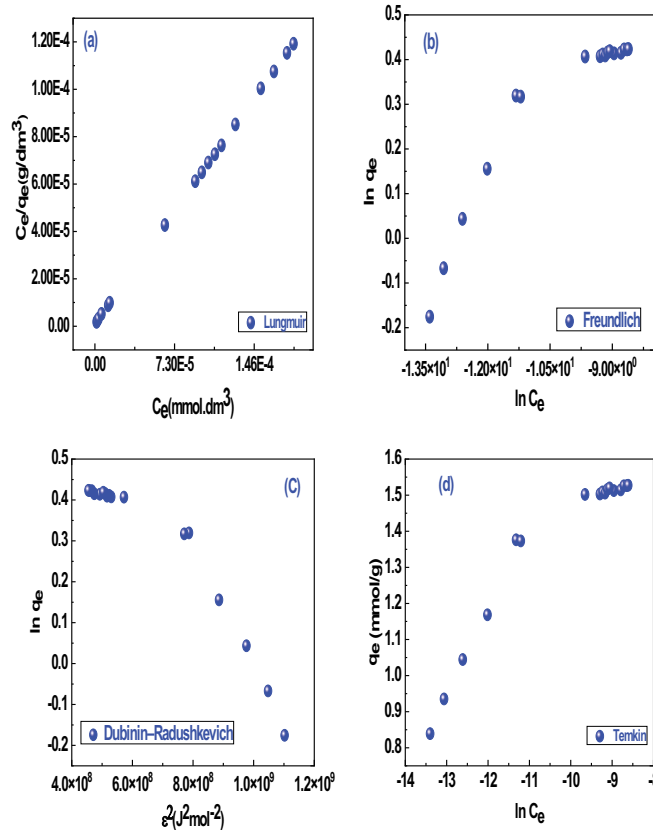
Fig. 9. Models for the linearized isothermal adsorption of TC onto NiO.

Table 2
Isotherms and their linear forms for TC adsorption on NiO nanoparticles [78,79]

Isotherm	Value of parameters	
Langmuir	$q_{m,exp}$ (mmol·g^{-1})	1.527
	q_m (mmol·g^{-1})	1.536
	K_L (L·mmol^{-1})	6.2E+05
	R^2	0.99952
Freundlich	N	9.362
	K_F (mmol·g^{-1})(L·mmol^{-1})$^{1/n}$	4.013
	R^2	0.877
Dubinin–Radushkevich	q_{DR}	0.834
	K_{DR} (J^2·mol^{-2})	−8.14E-10
	E_a (kJ·mol^{-1})	24.8
	R^2	0.9068
Temkin	b_T (L·mol^{-1})	19,081.73
	A_T (kJ·mol^{-1})	20.72
	R^2	0.91

Table 3
TC adsorption onto NiO nanoparticles: kinetic parameters and correlation factors [78,79]

Model	Value of parameters	
Pseudo-first-order kinetic	K_1 (min^{-1})	0.016
	q_e (mmol·g^{-1})	0.28
	R^2	0.822
Pseudo-second-order kinetic	K_2 (g·mg^{-1}·min^{-1})	7.49
	q_e (mmol·g^{-1})	1.49
	R^2	0.9999
Intraparticle diffusion	K_i (mg·g^{-1}·min$^{-1/2}$)	−0.069
	X (mg·g^{-1})	0.552
	R^2	0.1999
Elovich	β (g·mg^{-1})	−4.065
	α (mg·g^{-1}·min^{-1})	2.715
	R^2	0.3587
Experimental data	$q_{e,exp}$ (mmol·g^{-1})	1.4898

- The interaction between surfaces with various charges is how the electrostatic attraction is most frequently described. Tetracycline solution's cations and the anions on the NiO surface can easily establish ionic connections; this results in improved adsorption capacity [89].

- Dipole–dipole interactions called H-bonds are most frequently between two hydrogen atoms that are both donors and acceptors of hydrogen. It regularly keeps the performance of various organics adhering to NiO going. According to our model, the TC is where the hydrogen donor comes from (from –OH groups),
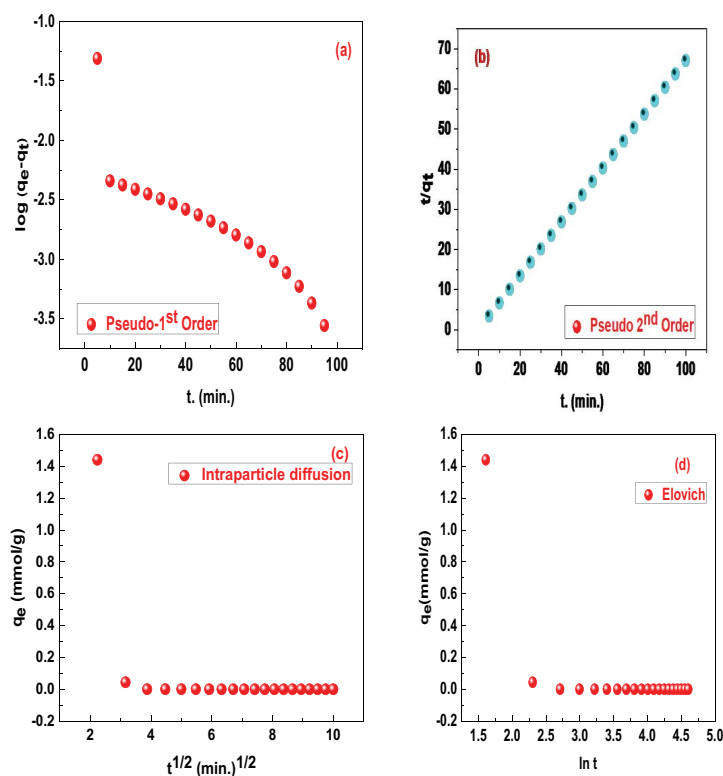
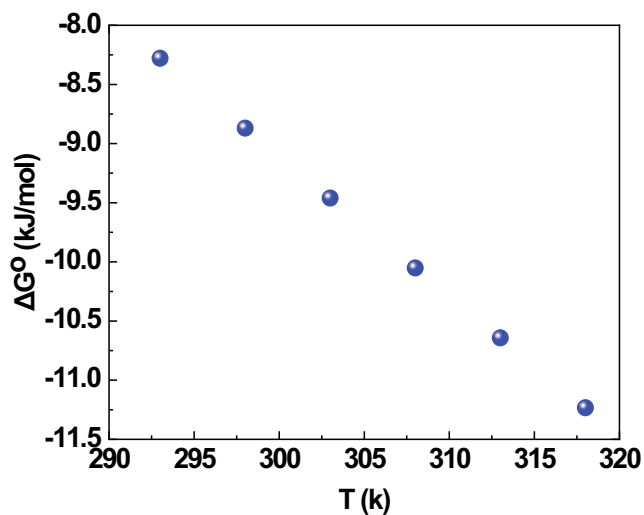Fig. 10. Linearized adsorption kinetic models for TC adsorption TC onto NiO.

Fig. 11. Graph displays how Gibb's free energy ($\Delta G°$) negativity increase with temperature (T).

In contrast, TC provides hydrogen acceptors (i.e., oxygen–nitrogen). The amount of hydrogen atoms in the TC and the nitrogen/oxygen components of the TC being examined are closely correlated with the strength of the H-bonding.

• TC was found to have aromatic ring that abundant with π-electrons, these led to form π–π interactions between NiO and TC.

• NiO's specific surface area and pore volume considerably decreased after adsorption, demonstrating that one of the mechanisms at play was pore filling analysis by BET supported this.

3.2.7.1. Active sites

The method of analyzing the adsorption groups the electrophilic/nucleophilic attacking region and the electrostatic potential zero zones in the investigated TC/NiO systems is referred to as molecular electrostatic potential (MEP). In this study, utilizing molecular electrostatic potentials, the entire electron density surface of TC was charted (MEP) (Fig. 13) [90].

On the other hand, have known active binding sites. As a result, if these groups are present, they will boost TC adsorption, yet the adsorption findings revealed the following: NiO adsorbent capacity in regards of ATC adsorption capacities is owing to that contact in between delocalized-electrons in NiO planes and free electrons in TC molecules positioned in aromatic rings or numerous bonds.

Table 5 shows the E_{HOMO} and E_{LUMO} principles, and the energy disparity between all compounds, $E_{LUMO-HOMO}$. The difference in energy can be used to find out how hard molecules are and how soft they are (Fig. 14). Because the molecule has a reduced volume of energy. It is more polarizable and less powerful (more reactive). TC quantum chemical descriptions were identified as chemical potential (μ), electronegativity (χ), global softness (б), global hardness (η) and electronegativity (χ), global hardness (б), global index of electrophilicity (ω) [41,42].
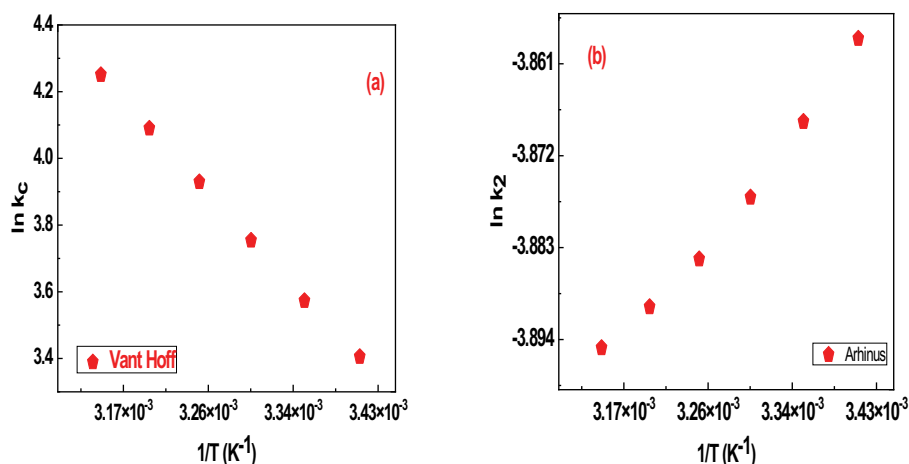
Fig. 12. (a) TC adsorption onto the NiO adsorbent is depicted via a van't Hoff plot. (b) TC adsorption onto the NiO adsorbent is depicted via an Arrhenius plot.

Table 4
$\Delta G°$, $\Delta H°$, and $\Delta S°$ for TC adsorption on NiO

Dye	T (K)	$\Delta H°$ (kJ·mol^{-1})	$\Delta S°$ (J·mol^{-1}·K^{-1})	E_a (kJ·mol^{-1})	T_0 (K)	$-\Delta G°$ (kJ·mol^{-1})
	298					8.27
	303					8.69
TC	308	26.35	118	1.15	223	9.46
	313					10.05
	318					11.23

Indeed, E_{gap} is theoretically characterized as a significant chemical component of TC that is highly reactive, a tiny gap denotes a high level of chemical reactivity (poor stable), a huge gap, on the other hand, suggests low chemical reactivity (highly stable) (Table 5).

3.2.8. Comparison with other adsorbents

Table 6 listing of the abilities of different sorbents for the sorption of TC demonstrates that sorbent's sorption capacity is significantly higher than that of other sorbents. Removal effectiveness might be improved because the sorbent's surface and its porous structure contain more active centers.

3.2.9. Desorption studies

Adsorbent's capacity to regenerate with its constancy are two important issues that influence its practical application. We've now compared NiO's adsorption potential over three adsorption–desorption cycles in a row [43]. The examined sorbent NiO was washed several times with ethanol until colorless, after that, distilled water was used to rinse it. At 60°C, the colorless NiO compound was dried overnight to achieve a constant weight. NiO is now prepared for the second-stage of absorption following renewal. The efficacy of regeneration was discovered
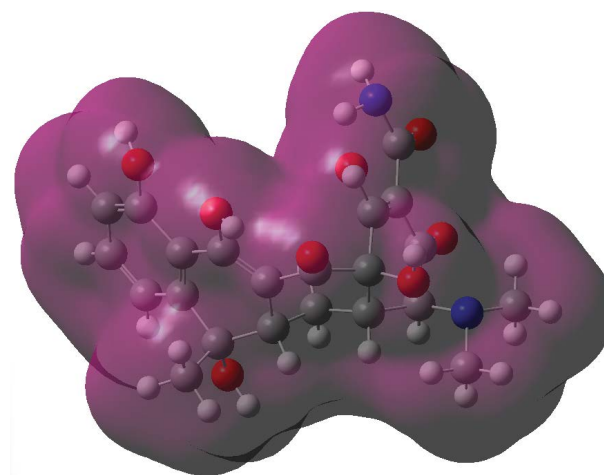

Fig. 13. Molecular electrostatic potential (MEP) for TC.

Table 5
Examined TC had its quantum chemical properties determined

Comp.	TC
E_{HOMO} (eV)	−0.2037
E_{LUMO} (eV)	−0.096
ΔE (eV)	0.1077
X (eV)	0.149
η (eV)	0.05
Pi (eV)	−0.15
σ (eV^{-1})	18.57
S (eV^{-1})	9.28
Ω (eV)	0.21
ΔN_{max}	2.78

to be 97.6%, 95.5%, 94.8%, 94% and 93.6% during each cycle of adsorption/desorption this could be because NiO absorptions are restricted. We used XRD to analyse the NiO material after three cycles of testing and found that

E_{HOMO}= -0.096

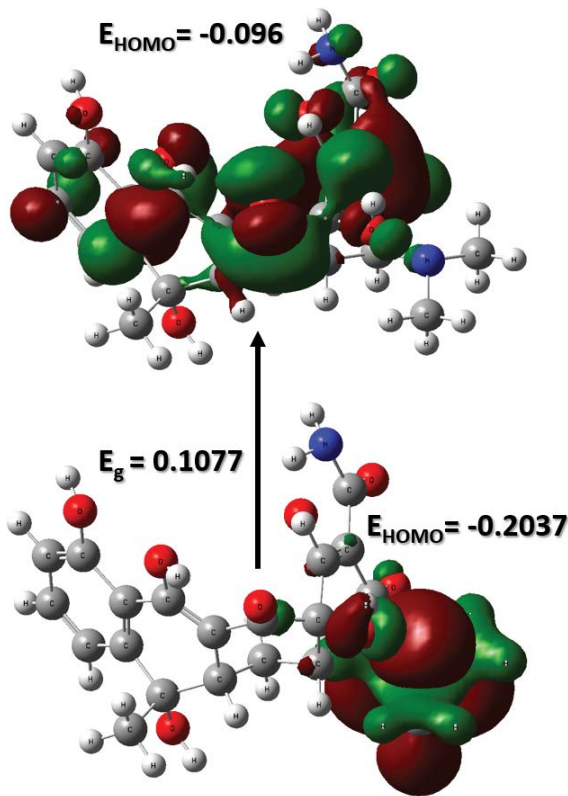E_g = 0.1077

E_{HOMO} = -0.2037

Fig. 14. TC optimized structures' molecular orbital density distribution at the Frontier.

the substance's crystallinity and structure had been preserved (Fig. 15). Findings show that NiO nanoparticles are highly recyclable. The following to evaluate the efficiency of the regeneration process, Eq. (4) was used.
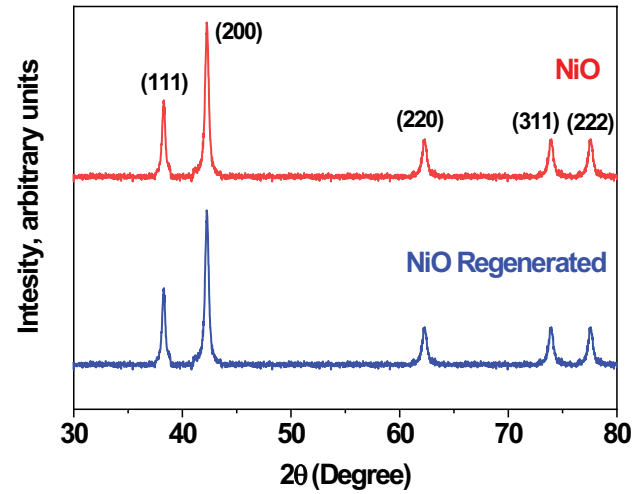

Fig. 15. XRD spectra of NiO at 450°C and NiO regenerated.

$$
\begin{aligned}
&\text{Regeneration efficiency}\,(\%)\\
&= \frac{\begin{array}{c}\text{Total capacity for adsorption}\\ \text{in the second run}\end{array}}{\begin{array}{c}\text{Total capacity for adsorption}\\ \text{in the Initial run}\end{array}} \times 100
\end{aligned}
\tag{4}
$$

4. Conclusions

A mesoporous nickel oxide was effectively created and characterized in the current investigation to remove and adsorb tetracycline from aqueous solution. The surface area was calculated to be 119.12 $m^2 \cdot g^{-1}$. The mesoporous nickel oxide exhibited good adsorption capacity toward 662 $mg \cdot g^{-1}$.

Table 6
Comparing the TC with NiO's ability to absorb water to that of other adsorbents

Adsorbents	Conditions		q_m (mg·g^{-1})	References
	pH	Temp.		
PAM/CA@Cu beads	5	303	356.57	[91]
Graphene oxide/calcium alginate composite fibers		298	131.57	[92]
3D alginate-based MOF hydrogel (MA-M)	8	298	364.89	[93]
Phenolic hydroxyl-derived copper alginate microspheres	7	318.5	199.14	[94]
Cu-immobilized alginate beads	3	318.5	58.57	[95]
Cu and Co nanoparticles co-doped MIL-101	4.8	318	161.86	[96]
Carboxymethyl-chitosan reformed montmorillonite		298	178.57	[97]
Cerium oxide nanoparticles		313	57.14	[98]
Alginate/reduced graphene oxide (rGO) double-network hydrogel (GAD)	8	298	290.70	[99]
Alginate/rGO single network hydrogel (GAS)	8	298	247.52	[99]
Alkali acid-modified magnetic biochar		298	97.96	[100]
MnFe$_2$O$_4$-embedded chitosan-diphenyl urea formaldehyde resin	6		172.12	[101]
Amino-Fe(III) functionalized SBA15	5		43.07	[102]
Fe$_3$O$_4$@SiO$_2$-chitosan/graphene oxide nanocomposite	6	298	110.22	[99]
NiO	7	298	662	This work

The adsorption isotherm was fitted to Langmuir whereas the adsorption kinetic was fit to a pseudo-second-order model, according to the findings. Adsorption had an energy of 24.8 kJ·mol^{-1}, indicating that chemisorption was the adsorption process. While during study the effect of temperature determine the thermodynamic parameter such as $\Delta G°$, $\Delta H°$, $\Delta S°$ from the data showed that the reaction was an endothermic, spontaneous reaction as the temperature increase the negativity $\Delta G°$, and removal efficiency were increase. Also study the possibility of the mechanism of interaction as it may be due to H-bonding, π–π interaction, prefilling or electrostatic interaction. The reusability of the NiO was checked for five cycle was 93.6 and this considered good advantage for using the NiO in TC removal.

Acknowledgment

References

[1] G.B. Dindaş, Y. Çalışkan, E.E. Celebi, M. Tekbaş, N. Bektaş, H. Cengiz Yatmaz, Treatment of pharmaceutical wastewater by combination of electrocoagulation, electro-Fenton and photocatalytic oxidation processes, J. Environ. Chem. Eng., 8 (2020) 103777, doi: 10.1016/j.jece.2020.103777.

[2] A. Yazidi, M. Atrous, F.E. Soetaredjo, L. Sellaoui, S. Ismadji, A. Erto, A. Bonilla-Petriciolet, G.L. Dotto, A.B. Lamine, Adsorption of amoxicillin and tetracycline on activated carbon prepared from durian shell in single and binary systems: experimental study and modeling analysis, Chem. Eng. J., 379 (2020) 122320, doi: 10.1016/j.cej.2019.122320.

[3] X. Bao, Z. Qiang, J.-H. Chang, W. Ben, J. Qu, Synthesis of carbon-coated magnetic nanocomposite (Fe$_3$O$_4$@C) and its application for sulfonamide antibiotics removal from water, J. Environ. Sci., 26 (2014) 962–969.

[4] X. Peng, F. Hu, F. Dai, Q. Xiong, C. Xu, Study of the adsorption mechanisms of ciprofloxacin antibiotics onto graphitic ordered mesoporous carbons, J. Taiwan Inst. Chem. Eng., 65 (2016) 472–481.

[5] M. Khraisheh, J. Kim, L. Campos, H. Ala'a, A. Al-Hawari, M. Al Ghouti, G.M. Walker, Removal of pharmaceutical and personal care products (PPCPs) pollutants from water by novel TiO$_2$–coconut shell powder (TCNSP) composite, J. Ind. Eng. Chem., 20 (2014) 979–987.

[6] Y. Lin, S. Xu, J. Li, Fast and highly efficient tetracyclines removal from environmental waters by graphene oxide functionalized magnetic particles, Chem. Eng. J., 225 (2013) 679–685.

[7] J. Hoslett, H. Ghazal, E. Katsou, H. Jouhara, The removal of tetracycline from water using biochar produced from agricultural discarded material, Sci. Total Environ., 751 (2021) 141755, doi: 10.1016/j.scitotenv.2020.141755.

[8] H. Sayğılı, F. Güzel, Effective removal of tetracycline from aqueous solution using activated carbon prepared from tomato (*Lycopersicon esculentum* Mill.) industrial processing waste, Ecotoxicol. Environ. Saf., 131 (2016) 22–29.

[9] R.S. Bangari, N. Sinha, Adsorption of tetracycline, ofloxacin and cephalexin antibiotics on boron nitride nanosheets from aqueous solution, J. Mol. Liq., 293 (2019) 111376, doi: 10.1016/j.molliq.2019.111376.

[10] A. Vona, F. Di Martino, J. Garcia-Ivars, Y. Picó, J.-A. Mendoza-Roca, M.-I. Iborra-Clar, Comparison of different removal techniques for selected pharmaceuticals, J. Water Process Eng., 5 (2015) 48–57.

[11] H.B. Quesada, A.T.A. Baptista, L.F. Cusioli, D. Seibert, C. de Oliveira Bezerra, R. Bergamasco, Surface water pollution by pharmaceuticals and an alternative of removal by low-cost adsorbents: a review, Chemosphere, 222 (2019) 766–780.

[12] M.R. Awual, A novel facial composite adsorbent for enhanced copper(II) detection and removal from wastewater, J. Chem. Eng. J., 266 (2015) 368–375.

[13] M.N. Hasan, M. Shenashen, M.M. Hasan, H. Znad, M.R. Awual, Assessing of cesium removal from wastewater using functionalized wood cellulosic adsorbent, Chemosphere, 270 (2021) 128668, doi: 10.1016/j.chemosphere.2020.128668.

[14] A.A. El-Bindary, M.G. El-Desouky, M.A.M. El-Afify, Thermal and spectroscopic studies of some prepared metal complexes and investigation of their potential anticancer and antiviral drug activity against SARS-CoV-2 by molecular docking simulation, Biointerface Res. Appl. Chem., 12 (2021) 1053–1075.

[15] S. Top, G.K. Akkaya, A. Demir, Ş. Yıldız, V. Balahorli, M.S. Bilgili, Investigation of leachate characteristics in field-scale landfill test cells, Int. J. Environ. Res., 13 (2019) 829–842.

[16] A. Daso, V. Nevondo, O. Okonkwo, T. Malehase, Leachate seepage from landfill: a source of groundwater mercury contamination in South Africa, Water SA, 45 (2019) 225–231.

[17] M.B. Yeamin, M.M. Islam, A.-N. Chowdhury, M.R. Awual, Efficient encapsulation of toxic dyes from wastewater using several biodegradable natural polymers and their composites, J. Cleaner Prod., 291 (2021) 125920, doi: 10.1016/j.jclepro.2021.125920.

[18] M. Naushad, A.A. Alqadami, A.A. Al-Kahtani, T. Ahamad, M.R. Awual, T. Tatarchuk, Adsorption of textile dye using para-aminobenzoic acid modified activated carbon: kinetic and equilibrium studies, J. Mol. Liq., 296 (2019) 112075, doi: 10.1016/j.molliq.2019.112075.

[19] F. Gamoń, M. Tomaszewski, A. Ziembińska-Buczyńska, Ecotoxicological study of landfill leachate treated in the ANAMMOX process, Water Qual. Res. J., 54 (2019) 230–241.

[20] E.C. Baettker, C. Kozak, H.G. Knapik, M.M. Aisse, Applicability of conventional and non-conventional parameters for municipal landfill leachate characterization, Chemosphere, 251 (2020) 126414, doi: 10.1016/j.chemosphere.2020.126414.

[21] A.G. King, Research advances: caught on tape: catalyst recovery; secondary structure switch; DNA-based chiral catalysts, J. Chem. Educ., 83 (2006) 10, doi: 10.1021/ed083p10.

[22] Y.-J. Wang, D.-A. Jia, R.-J. Sun, H.-W. Zhu, D.-M. Zhou, Adsorption and cosorption of tetracycline and copper(II) on montmorillonite as affected by solution pH, Environ. Sci. Technol., 42 (2008) 3254–3259.

[23] J.-C. David, A. Buchet, J.-N. Sialelli, S. Delouvée, The use of antibiotics in veterinary medicine: representations of antibiotics and biosecurity by pig farmers, Pratiques Psychologiques, 27 (2021) 159–170.

[24] Y. Zhu, K. Liu, J. Zhang, X. Liu, L. Yang, R. Wei, S. Wang, D. Zhang, S. Xie, F. Tao, Antibiotic body burden of elderly Chinese population and health risk assessment: a human biomonitoring-based study, Environ. Pollut., 256 (2020) 113311, doi: 10.1016/j.envpol.2019.113311.

[25] Y. Yang, L. Bian, X. Hang, C. Yan, Y. Huang, F. Ye, G. Zhang, G. Jin, H. Bi, In vitro activity of new tetracycline analogues omadacycline and eravacycline against clinical isolates of *Helicobacter pylori* collected in China, Diagn. Microbiol. Infect. Dis., 98 (2020) 115129, doi: doi: 10.1016/j.diagmicrobio.2020.115129.

[26] R. Chan, S. Wandee, M. Wang, W. Chiemchaisri, C. Chiemchaisri, C. Yoshimura, Fate, transport and ecological risk of antibiotics from pig farms along the Bang Pakong River, Thailand, Agric. Ecosyst. Environ., 304 (2020) 107123, doi: 10.1016/j.agee.2020.107123.

[27] L. Ji, W. Chen, J. Bi, S. Zheng, Z. Xu, D. Zhu, P.J. Alvarez, Adsorption of tetracycline on single-walled and multi-walled carbon nanotubes as affected by aqueous solution chemistry, Environ. Toxicol. Chem., 29 (2010) 2713–2719.

[28] R. Li, Q. Yuan, Y. Zhang, J. Ling, T. Han, Hydrophilic interaction chromatographic determination of oxytetracycline in the environmental water using silica column, J. Liq. Chromatogr. Related Technol., 34 (2011) 511–520.

[29] H. Sun, X. Shi, J. Mao, D. Zhu, Tetracycline sorption to coal and soil humic acids: an examination of humic structural heterogeneity, Environ. Toxicol. Chem., 29 (2010) 1934–1942.

[30] S. Mishra, D. Tiwary, A. Ohri, A.K. Agnihotri, Impact of municipal solid waste landfill leachate on groundwater quality in Varanasi, India, Groundwater Sustainable Dev., 9 (2019) 100230, doi: 10.1016/j.gsd.2019.100230.

[31] A. Mittal, R. Singh, S. Chakma, G. Goel, Permeable reactive barrier technology for the remediation of groundwater contaminated with nitrate and phosphate resulted from pit-toilet leachate, J. Water Process Eng., 37 (2020) 101471, doi: 10.1016/j.jwpe.2020.101471.

[32] T. Rasheed, M. Bilal, A.A. Hassan, F. Nabeel, R.N. Bharagava, L.F.R. Ferreira, H.N. Tran, H.M. Iqbal, Environmental threatening concern and efficient removal of pharmaceutically active compounds using metal-organic frameworks as adsorbents, Environ. Res., 185 (2020) 109436, doi: 10.1016/j.envres.2020.109436.

[33] Gh.H. Al-Hazmi, M.S. Refat, M.G. El-Desouky, A.A. El-Bindary, Effective adsorption and removal of industrial dye from aqueous solution using mesoporous zinc oxide nanoparticles via metal organic frame work: equilibrium, kinetics and thermodynamic studies, Desal. Water Treat., 272 (2022) 277–289.

[34] M. Feng, L. Yan, X. Zhang, P. Sun, S. Yang, L. Wang, Z. Wang, Fast removal of the antibiotic flumequine from aqueous solution by ozonation: influencing factors, reaction pathways, and toxicity evaluation, Sci. Total Environ., 541 (2016) 167–175.

[35] J. Gomes, R. Costa, R.M. Quinta-Ferreira, R.C. Martins, Application of ozonation for pharmaceuticals and personal care products removal from water, Sci. Total Environ., 586 (2017) 265–283.

[36] M. Klavarioti, D. Mantzavinos, D. Kassinos, Removal of residual pharmaceuticals from aqueous systems by advanced oxidation processes, Environ. Int., 35 (2009) 402–417.

[37] E. Hapeshi, A. Achilleos, M.I. Vasquez, C. Michael, N.P. Xekoukoulotakis, D. Mantzavinos, D. Kassinos, Drugs degrading photocatalytically: kinetics and mechanisms of ofloxacin and atenolol removal on titania suspensions, Water Res., 44 (2010) 1737–1746.

[38] R. Hao, X. Xiao, X. Zuo, J. Nan, W. Zhang, Efficient adsorption and visible-light photocatalytic degradation of tetracycline hydrochloride using mesoporous BiOI microspheres, J. Hazard. Mater., 209 (2012) 137–145.

[39] J. Niu, Y. Xie, H. Luo, Q. Wang, Y. Zhang, Y. Wang, Cobalt oxide loaded graphitic carbon nitride as adsorptive photocatalyst for tetracycline removal from aqueous solution, Chemosphere, 218 (2019) 169–178.

[40] W. Yang, Y. Wu, L. Zhang, J. Jiang, L. Feng, Removal of five selected pharmaceuticals by coagulation in the presence of dissolved humic acids and kaolin, Desal. Water Treat., 54 (2015) 1134–1140.

[41] S.M. Khalaf, S.M. Al-Mahmoud, Adsorption of tetracycline antibiotic from aqueous solutions using natural Iraqi bentonite, Egypt. J. Chem., 64 (2021) 3–4.

[42] G.Z. Kyzas, J. Fu, N.K. Lazaridis, D.N. Bikiaris, K.A. Matis, New approaches on the removal of pharmaceuticals from wastewaters with adsorbent materials, J. Mol. Liq., 209 (2015) 87–93.

[43] N. Dhiman, N. Sharma, Removal of pharmaceutical drugs from binary mixtures by use of ZnO nanoparticles: (competitive adsorption of drugs), Environ. Technol. Innovation, 15 (2019) 100392, doi: 10.1016/j.eti.2019.100392.

[44] M.G. El-Desouky, M.A. Khalil, A.A. El-Bindary, M.A. El-Bindary, Biological, biochemical and thermochemical techniques for biofuel production: an updated review, Biointerface Res. Appl. Chem., 12 (2022) 3034–3054.

[45] M.G. El-Desouky, M. Abd El-Wahab, A.A. El-Bindary., Interpretations and DFT calculations for polypropylene/cupper oxide nanosphere, Biointerface Res. Appl. Chem., 12 (2021) 1134–1147.

[46] MG. El-Desouky, AA. El-Bindary, MAM. El-Afify, N. Hassan, Synthesis, characterization, theoretical calculation, DNA binding, molecular docking, anticovid-19 and anticancer chelation studies of some transition metal complexes, Inorg. Nano-Metal Chem., 52 (2022) 1–16.

[47] N. Hassan, A. El-Sonbati, M. El-Desouky, Synthesis, characterization, molecular docking and DNA binding studies of Cu(II), Ni(II), Zn(II) and Mn(II) complexes, J. Mol. Liq., 242 (2017) 293–307.

[48] N. Hassan, A. Shahat, A. El-Didamony, M. El-Desouky, A. El-Bindary, Synthesis and characterization of ZnO nanoparticles via zeolitic imidazolate framework-8 and its application for removal of dyes, J. Mol. Struct., 1210 (2020) 128029, doi: 10.1016/j.molstruc.2020.128029.

[49] N. Hassan, A. Shahat, A. El-Didamony, M. El-Desouky, A. El-Bindary, Mesoporous iron oxide nano spheres for capturing organic dyes from water sources, J. Mol. Struct., 1217 (2020) 128361, doi: 10.1016/j.molstruc.2020.128361.

[50] G.A. Al-Hazmi, A.A. El-Zahhar, M.G. El-Desouky, M.A. El-Bindary, A.A. El-Bindary, Adsorption of industrial dye onto a zirconium metal-organic framework: synthesis, characterization, kinetics, thermodynamics, and DFT calculations, J. Coord. Chem., 75 (2022) 1203–1229.

[51] G.H. Al-Hazmi, M.G. El-Desouky, A.A. El-Bindary, Synthesis, characterization and microstructural evaluation of ZnO nanoparticles by William–Hall and size-strain plot methods, Bull. Chem. Soc. Ethiop., 36 (2022) 815–829.

[52] S. Khandaker, M.F. Chowdhury, M.R. Awual, A. Islam, T. Kuba, Efficient cesium encapsulation from contaminated water by cellulosic biomass based activated wood charcoal, Chemosphere, 262 (2021) 127801, doi: 10.1016/j.chemosphere.2020.127801.

[53] K.T. Kubra, M.S. Salman, M.N. Hasan, A. Islam, S.H. Teo, M.M. Hasan, M.C. Sheikh, M.R. Awual, Sustainable detection and capturing of cerium(III) using ligand embedded solid-state conjugate adsorbent, J. Mol. Liq., 338 (2021) 116667, doi: 10.1016/j.molliq.2021.116667.

[54] M.R. Awual, A facile composite material for enhanced cadmium(II) ion capturing from wastewater, J. Environ. Chem. Eng., 7 (2019) 103378, doi: 10.1016/j.jece.2019.103378.

[55] H.M. Munjur, M.N. Hasan, M.R. Awual, M.M. Islam, M. Shenashen, Iqbal, Biodegradable natural carbohydrate polymeric sustainable adsorbents for efficient toxic dye removal from wastewater, J. Mol. Liq., 319 (2020) 114356, doi: 10.1016/j.molliq.2020.114356.

[56] M.S. Frost, M.J. Dempsey, D.E. Whitehead, The response of citrate functionalised gold and silver nanoparticles to the addition of heavy metal ions, Colloids Surf., A, 518 (2017) 15–24.

[57] K.T. Kubra, M.S. Salman, M.N. Hasan, A. Islam, M.M. Hasan, M.R. Awual, Utilizing an alternative composite material for effective copper(II) ion capturing from wastewater, J. Mol. Liq., 336 (2021) 116325, doi: 10.1016/j.molliq.2021.116325.

[58] M.A. Islam, M.J. Angove, D.W. Morton, B.K. Pramanik, M.R. Awual, A mechanistic approach of chromium(VI) adsorption onto manganese oxides and boehmite, J. Environ. Chem. Eng., 8 (2020) 103515, doi: 10.1016/j.jece.2019.103515.

[59] M.M. Rahman, T.A. Sheikh, A.M. Asiri, M.R. Awual, Development of 3-methoxyaniline sensor probe based on thin $Ag_2O@La_2O_3$ nanosheets for environmental safety, New J. Chem., 43 (2019) 4620–4632.

[60] A. Fouda, S.S. Salem, A.R. Wassel, M.F. Hamza, Th.I. Shaheen, Optimization of green biosynthesized visible light active CuO/ZnO nano-photocatalysts for the degradation of organic methylene blue dye, Heliyon, 6 (2020) e04896, doi: 10.1016/j.heliyon.2020.e04896.

[61] F. Ramezani, R. Zare-Dorabei, Simultaneous ultrasonic-assisted removal of malachite green and methylene blue from aqueous solution by Zr-SBA-15, Polyhedron, 166 (2019) 153–161.

[62] M.G. El-Desouky, A. Shahat, A.A. El-Bindary, M.A. El-Bindary, Description, kinetic and equilibrium studies of the adsorption of carbon dioxide in mesoporous iron oxide nanospheres, Biointerface Res. Appl. Chem., 12 (2021) 1022–1038.

[63] M.S. Tehrania, R. Zare-Dorabei, Highly efficient simultaneous ultrasonic-assisted adsorption of methylene blue and rhodamine B onto metal organic framework MIL-68 (Al): central composite design optimization, RSC Adv., 6 (2016) 27416–27425.

[64] F.K. Mostafapour, M. Yilmaz, A.H. Mahvi, A. Younesi, F. Ganji, D.J.D. Balarak, Adsorptive removal of tetracycline from aqueous solution by surfactant-modified zeolite: equilibrium, kinetics and thermodynamics, Desal. Water Treat., 247 (2022) 216–228.

[65] D. Balarak, A.H. Mahvi, M.J. Shim, S.-M. Lee, Adsorption of ciprofloxacin from aqueous solution onto synthesized NiO: isotherm, kinetic and thermodynamic studies, Desal. Water Treat., 212 (2021) 390–400.

[66] A.S. Al-Wasidi, I.I. AlZahrani, A.M. Naglah, M.G. El-Desouky, M.A. Khalil, A.A. El-Bindary, M.A. El-Bindary, Effective removal of methylene blue from aqueous solution using metal-organic framework; modelling analysis, statistical physics treatment and DFT calculations, ChemistrySelect, 6 (2021) 11431–11447.

[67] M.S. Tehrani, R. Zare-Dorabei, Competitive removal of hazardous dyes from aqueous solution by MIL-68(Al): derivative spectrophotometric method and response surface methodology approach, Spectrochim. Acta, Part A, 60 (2016) 8–18.

[68] G.A.A. Al-Hazmi, M.A. El-Bindary, M.G. El-Desouky, A.A. El-Bindary, Efficient adsorptive removal of industrial dye from aqueous solution by synthesized zeolitic imidazolate framework-8 loaded date seed activated carbon and statistical physics modeling, Desal. Water Treat., 258 (2022) 85–103.

[69] A.A. Mohammadi, A. Zarei, H. Alidadi, M. Afsharnia, M. Shams, Two-dimensional zeolitic imidazolate framework-8 for efficient removal of phosphate from water, process modeling, optimization, kinetic, and isotherm studies, Desal. Water Treat., 129 (2018) 244–254.

[70] I. Langmuir, The adsorption of gases on plane surfaces of glass, mica and platinum, J. Am. Chem. Soc., 40 (1918) 1361–1403.

[71] H. Freundlich, W. Heller, The adsorption of cis- and *trans*-azobenzene, J. Am. Chem. Soc., 61 (1939) 2228–2230.

[72] M.J. Temkin, V. Pyzhev, Recent modifications to Langmuir isotherms, Acta Phys. Chem., 12 (1940) 217–222.

[73] M.M. Dubinin, E. Zaverina, L. Radushkevich, Sorption and structure of active carbons. I. Adsorption of organic vapors, Zh. Fiz. Khim., 21 (1947) 151–162.

[74] T.A. Altalhi, M.M. Ibrahim, G.A.M. Mersal, M.H.H. Mahmoud, T. Kumeria, M.G. El-Desouky, A.A. El-Bindary, M.A. El-Bindary, Adsorption of doxorubicin hydrochloride onto thermally treated green adsorbent: equilibrium, kinetic and thermodynamic studies, J. Mol. Struct., 1263 (2022) 133160, doi: 10.1016/j.molstruc.2022.133160.

[75] D. Balarak, M. Baniasadi, S.-M. Lee, M.J. Shim, Ciprofloxacin adsorption onto *Azolla filiculoides* activated carbon from aqueous solutions, Desal. Water Treat., 218 (2021) 444–453.

[76] D. Balarak, Z. Taheri, M.J. Shim, S.-M. Lee, C. Jeon, Adsorption kinetics and thermodynamics and equilibrium of ibuprofen from aqueous solutions by activated carbon prepared from *Lemna minor*, Desal. Water Treat., 215 (2021) 183–193.

[77] A.D. Khatibi, A.H. Mahvi, N. Mengelizadeh, D. Balarak, Adsorption–desorption of tetracycline onto molecularly imprinted polymer: isotherm, kinetics, and thermodynamics studies, Desal. Water Treat., 230 (2021) 240–251.

[78] M. El-Desouky, M. El-Bindary, A. El-Bindary, Effective adsorptive removal of anionic dyes from aqueous solution, Vietnam J. Chem., 59 (2021) 341–361.

[79] M. El-Bindary, M.G. El-Desouky, A.A. El-Bindary, Adsorption of industrial dye from aqueous solutions onto thermally treated green adsorbent: a complete batch system evaluation, J. Mol. Liq., 346 (2021) 117082, doi: 10.1016/j.molliq.2021.117082.

[80] S.K. Lagergren, About the theory of so-called adsorption of soluble substances, Sven. Vetenskapsakad. Handingarl, 24 (1898) 1–39.

[81] Y.-S. Ho, G. McKay, Sorption of dye from aqueous solution by peat, Chem. Eng. J., 70 (1998) 115–124.

[82] D. Karataş, D. Senol-Arslan, O. Ozdemir, Experimental and atomic modeling of the adsorption of acid azo dye 57 to sepiolite, Clays Clay Miner., 66 (2018) 426–437.

[83] M.A. El-Bindary, M.G. El-Desouky, A.A. El-Bindary, Metal–organic frameworks encapsulated with an anticancer compound as drug delivery system: synthesis, characterization, antioxidant, anticancer, antibacterial and molecular docking investigation, Appl. Organomet. Chem., 36 (2022) e6660, doi: 10.1002/aoc.6660.

[84] M. El-Desouky, A. El-Bindary, Magnetic metal-organic framework (Fe_3O_4@ZIF-8) nanocomposites for adsorption of anionic dyes from wastewater, Inorg. Nano-Metal Chem., (2021) 1–15.

[85] G. Mohamed, N. Hassan, A. Shahat, A. El-Didamony, A. Ashraf, Synthesis and characterization of porous magnetite nanosphere iron oxide as a novel adsorbent of anionic dyes removal from aqueous solution, Biointerface Res. Appl. Chem., 11 (2021) 13377–13401.

[86] N.C. Corda, M.S. Kini, A review on adsorption of cationic dyes using activated carbon, MATEC Web Conf., 144 (2018) 02022.

[87] G.A.A. AlHazmi, Kh.S. AbouMelha, M.G. El-Desouky, A.A. El-Bindary, Effective adsorption of doxorubicin hydrochloride on zirconium metal-organic framework: equilibrium, kinetic and thermodynamic studies, J. Mol. Struct., 1258 (2022) 132679, doi: 10.1016/j.molstruc.2022.132679.

[88] G.A. Al-Hazmi, A.A. El-Zahhar, M.G. El-Desouky, M.A. El-Bindary, A.A. El-Bindary, Efficiency of Fe_3O_4@ZIF-8 for the removal of doxorubicin from aqueous solutions: equilibrium, kinetics and thermodynamic studies, J. Environ. Technol., (2022) 1–48.

[89] A.M. Elgarahy, A. Akhdhar, A.S. Al-Bogami, K.Z. Elwakeel, Magnetically separable solid phase extractor for static anionic dyes adsorption from aqueous solutions, Surf. Interfaces, 30 (2022) 101962, doi: 10.1016/j.surfin.2022.101962.

[90] A.S. Al-Wasidi, I.I. AlZahrani, H.I. Thawibaraka, A.M. Naglah, M.G. El-Desouky, M.A. El-Bindary, Adsorption studies of carbon dioxide and anionic dye on green adsorbent, J. Mol. Struct., 1250 (2022) 131736, doi: 10.1016/j.molstruc.2021.131736.

[91] H. Luo, Y. Liu, H. Lu, Q. Fang, H. Rong, Efficient adsorption of tetracycline from aqueous solutions by modified alginate beads after the removal of Cu(II) ions, ACS Omega, 6 (2021) 6240–6251.

[92] H. Zhu, T. Chen, J. Liu, D. Li, Adsorption of tetracycline antibiotics from an aqueous solution onto graphene oxide/calcium alginate composite fibers, RSC Adv., 8 (2018) 2616–2621.

[93] Y. Zhuang, Y. Kong, X. Wang, B. Shi, Novel one step preparation of a 3D alginate based MOF hydrogel for water treatment, New J. Chem., 43 (2019) 7202–7208.

[94] X. Zhang, X. Lin, Y. He, X. Luo, Phenolic hydroxyl derived copper alginate microspheres as superior adsorbent for effective adsorption of tetracycline, Int. J. Biol. Macromol., 136 (2019) 445–459.

[95] X. Zhang, X. Lin, Y. He, Y. Chen, X. Luo, R. Shang, Study on adsorption of tetracycline by Cu-immobilized alginate adsorbent from water environment, Int. J. Biol. Macromol., 124 (2019) 418–428.

[96] J. Jin, Z. Yang, W. Xiong, Y. Zhou, R. Xu, Y. Zhang, J. Cao, X. Li, C. Zhou, Cu and Co nanoparticles co-doped MIL-101 as a novel adsorbent for efficient removal of tetracycline from aqueous solutions, Sci. Total Environ., 650 (2019) 408–418.

[97] J. Ma, Y. Lei, M.A. Khan, F. Wang, Y. Chu, W. Lei, M. Xia, S. Zhu, Adsorption properties, kinetics & thermodynamics of tetracycline on carboxymethyl-chitosan reformed montmorillonite, Int. J. Biol. Macromol., 124 (2019) 557–567.

[98] I. Nurhasanah, V. Gunawan, H. Sutanto, Cerium oxide nanoparticles application for rapid adsorptive removal of tetracycline in water, J. Environ. Chem. Eng., 8 (2020) 103613, doi: 10.1016/j.jece.2019.103613.

[99] Y. Zhuang, F. Yu, J. Ma, J. Chen, Enhanced adsorption removal of antibiotics from aqueous solutions by modified alginate/graphene double network porous hydrogel, J. Colloid Interface Sci., 507 (2017) 250–259.

[100] J. Dai, X. Meng, Y. Zhang, Y. Huang, Effects of modification and magnetization of rice straw derived biochar on adsorption of tetracycline from water, Bioresour. Technol., 311 (2020) 123455, doi: 10.1016/j.biortech.2020.123455.

[101] T. Ahamad, A.A. Chaudhary, M. Naushad, S.M. Alshehri, Fabrication of $MnFe_2O_4$ nanoparticles embedded chitosan-diphenylureaformaldehyde resin for the removal of tetracycline from aqueous solution, Int. J. Biol. Macromol., 134 (2019) 180–188.

[102] Z. Zhang, H. Lan, H. Liu, J. Qu, Removal of tetracycline antibiotics from aqueous solution by amino-Fe(III) functionalized SBA15, Colloids Surf., A, 471 (2015) 133–138.

Supporting information

S1. Materials and methods

S1.1. Chemicals and instruments

Here, the chemicals used are of pure grade in this analysis and used without purification Table 1. Sigma-Aldrich Chemical Corporation, USA, purchased dimethyl sulfoxide (DMSO) ($NiCl_2$).

S1.2. Synthesis of 3-acetyl-7-hydroxycoumarin

The ligand hydroxycoumarin (HL) was prepared by two steps (Fig. S1):

Step 1

3-methoxycarbonyl-7-hydroxycoumarin (0.01 mol) was prepared via the condensation of 2,4-dihydroxy-benzaldehyde with dimethyl malonate in the presence of piperidine. The medium temperature should be maintained at 5°C by using an ice salt bath during addition, and then the reaction mixture was kept at room temperature overnight, and then poured with vigorous stirring into a

Table S1
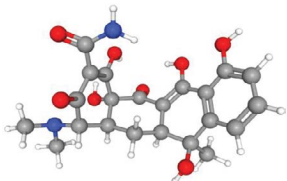Adsorbate tetracycline characteristics used in the research

Compound	Ball and stick model of tetracycline	Molar mass (g·mol⁻¹)	λ_{max}
Tetracycline		444.4	529 nm

Table S2
List of instruments

Type of analysis	Models
X-ray diffraction	Crysfire and Chekcell computer databases
Transmission electron microscopy (TEM)	TEM, FEI Tecnai G² F20, USA
Fourier-transform infrared spectroscopy (FTIR) spectra	Jasco FTIR-4100 spectrophotometer (Australia)
UV-visible spectrophotometer	Hach Lange DR5000 (HACH LANGE GmbH, Germany)
Brunauer–Emmett–Teller	ASAP 2020 (Micromeritics, USA)
Scanning electron microscope	JEOL JSM-6510 LV (Japan)
pH meter	Hanna (Model 211), Hanna Instruments, Romania

mixture crushed ice and water. The solid 3-methoxy carbonyl-7-hydroxycoumarin (Fig. S1) was filtered off and washed several times with cold water and recrystallized from ethanol. Elemental analysis: $C_{11}H_8O_4$ (M = 204.19) C 64.4 (calc. 64.7); H 3.92 (3.96); O 34.38 (31.34) % IR (KBr): 3,430 υ(OH), 1,668 υ(C=O) cm⁻¹ hydrogen-1 nuclear magnetic resonance (¹H NMR).

S2. Materials and apparatus

Spectroscopic level was obtained from Sigma-Aldrich (USA), Fluka (India) and Merck (Germany) from all the reagents and solvents. All the apparatus used are discussed in our previous work [1]

S2.1. Synthesis of 3-cyano-7-hydroxycoumarin

Step 1

3-Cyano-7-hydroxycoumarin (0.01 mol) was prepared [2] via the condensation of 2,4-dihydroxybenzaldehyde with ethyl cyano acetate in the existence of the piperidine. The medium temperature should be maintained at 5°C by using ice salt bath during addition, and the reaction mixture was then kept overnight at room temperature., and then poured in a mixture of crushed ice and water with vigorous stirring. The solid 3-cyano-7-hydroxycoumarin (Fig. S1) was filtered off and washed several times with cold water and recrystallized from ethanol. Elemental analysis: $C_{10}H_5O_3N$ (M = 187.16) C 64.25 (calc. 64.17); H 2.77 (2.70); N 7.55 (7.49) % IR (KBr): 3,430 υ(OH), 2,330 υ(C≡N), 1,668 υ(C=O) cm⁻¹. ¹H NMR in DMSO, internal tetramethyl silane, d (ppm): δ 1.5 (t, 3H, CH_3), 4.25 (q, 2H, CH_2), 6.77–7.93 (m, 7H, Ar-H), 8.70 (s, 1H, OH) ppm.

Step 2

A solution that is well stirred chloroaniline (0.01 mol) in an ice bath, 10 mL ethanol and 5 mL 2 M HCl were cooled and diazotized with an aqueous sodium nitrite solution (5 mL, 0.01 mol). The cooled (0°C–5°C) diazonium solution has been wisely added to a well stirred solution to drop (0.01 mol) 3-cyano-7-hydroxycoumarin in (100 mL) ethanol has sodium hydroxide (0.01 mol) during 45 min. The mixture was blended for a further 30 min and then left in the fridge for 2 h (Fig. S1). The solid product was collected, washed with water, dried and ethanol-recrystallized.

S2.2. Synthesis of solid complexes

Ni the complex was prepared (Fig. S2) by refluxing 1 mmol of the ligand under investigation with 1 mmol of the metal salt ($NiCl_2·6H_2O$) in an ethanolic solution in the water bath for 3 h. The pH of the solution was maintained at a value of 5–6 by the addition of dilute ammonia solution (10 wt.%). The resulting solid complexes were filtered off, washed several times with absolute ethanol, and finally dried in a vacuum desiccator over anhydrous calcium chloride.

Table S3
List of abbreviation

Symbol	Definition
q_e	Adsorbed amount of dye at equilibrium concentration, $mmol \cdot g^{-1}$
$q_m L$	Maximum sorption capacity (corresponding to the saturation of the monolayer, $mmol \cdot g^{-1}$)
K_L	Langmuir binding constant which is related to the energy of sorption, $L \cdot mmol^{-1}$
C_e	Equilibrium concentration of dyes in solution
K_F	Freundlich constants related to the sorption capacity, $(mmol \cdot g^{-1})(L \cdot mmol^{-1})^{1/n}$
n	Intensity
K_{DR}	constant related to the sorption energy, $J^2 \cdot mol^{-2}$
q_{DR}	Theoretical saturation capacity, $mmol \cdot g^{-1}$
ε	Polanyi potential, $J^2 \cdot mol^{-2}$
R	Gas constant, $8.314\ J \cdot mol^{-1} \cdot K^{-1}$
T	Temperature where the adsorption occurs
A_T	Temkin isotherm constant
b_T	Temkin constant in relation to heat of adsorption, $J \cdot mol^{-1}$
q_t	Amount of dye adsorbed, $mmol \cdot g^{-1}$
K_1	Rate constant for pseudo-first-order constant for the adsorption processes, min^{-1}
q_2	Maximum adsorption capacity for pseudo-second-order
K_2	Rate constant for pseudo-first-order constant for the adsorption processes, $g \cdot mg^{-1} \cdot min^{-1}$
α	Chemical adsorption rate, $mg \cdot g^{-1} \cdot min^{-1}$
β	Coefficient in relation with extension of covered surface
$\Delta G°$	Free Gibb's energy
$\Delta H°$	Enthalpy
$\Delta S°$	Entropy
K_c	Distribution coefficient
C_{eq}	Concentration at equilibrium, $mg \cdot L^{-1}$
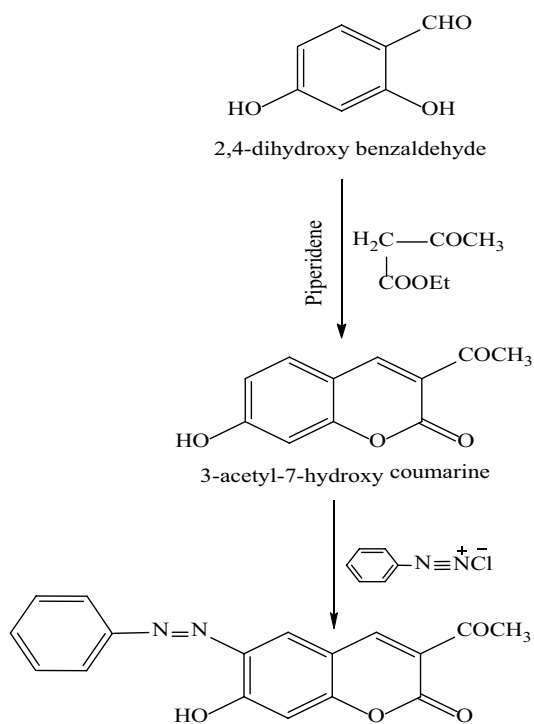
Fig. S1. Structure for the preparation acetyl-6-(phenyl azo)-7-hydroxycoumarin.

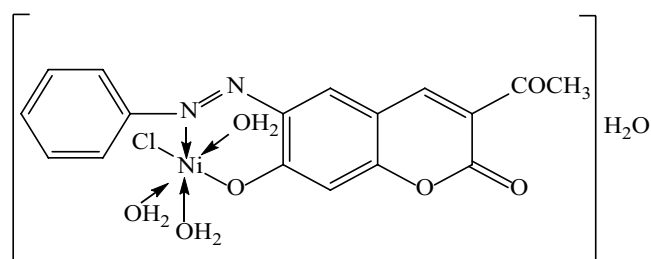Fig. S2. [Ni(L)Cl(OH$_2$)$_3$]H$_2$O complex.
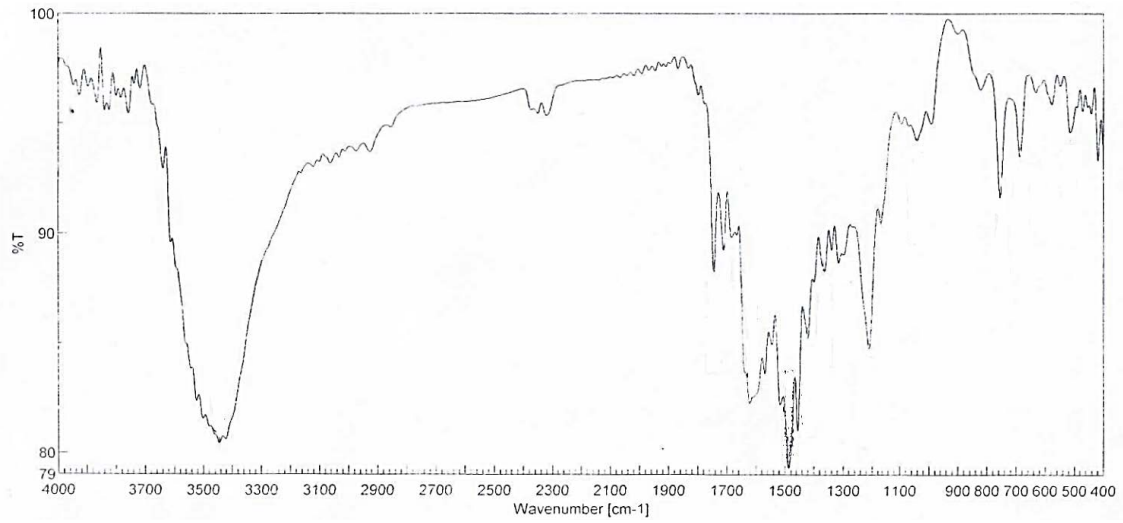
Fig. S3. IR spectra of [NiLCl(OH$_2$)$_3$].
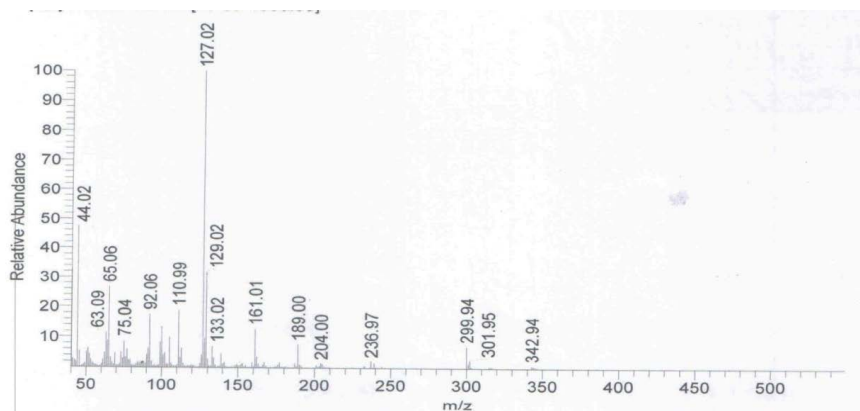
Fig. S4. Mass spectrum of [NiLCl(OH$_2$)$_3$].
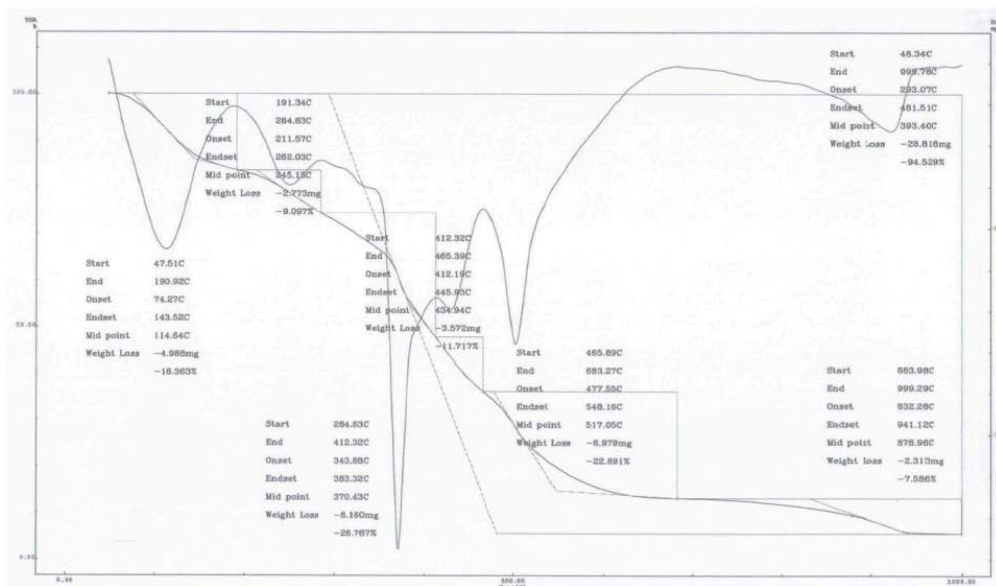
Fig. S5. Thermal analysis curves (TGA, DTG) of [NiLCl(OH$_2$)$_3$].